The Journal of Chemical Physics

Membrane potential sensing: Material design and method development for single particle optical electrophysiology

Cite as: J. Chem. Phys. **156**, 084201 (2022); https://doi.org/10.1063/5.0076522
Submitted: 26 October 2021 • Accepted: 26 January 2022 • Accepted Manuscript Online: 27 January 2022 • Published Online: 22 February 2022

Debjit Roy, Zehavit Shapira and Shimon Weiss

The Journal of Chemical Physics REVIEW scitation.org/journal/jcp

Membrane potential sensing: Material design and method development for single particle optical electrophysiology

Cite as: J. Chem. Phys. 156, 084201 (2022); doi: 10.1063/5.0076522
Submitted: 26 October 2021 • Accepted: 26 January 2022 •
Published Online: 22 February 2022

Debjit Roy,[1,2] Zehavit Shapira,[3,4] and Shimon Weiss[1,3,4,5,a)]

AFFILIATIONS

[1] Department of Chemistry and Biochemistry, University of California Los Angeles, Los Angeles, California 90095, USA
[2] UCLA-DOE Institute for Genomics and Proteomics, University of California Los Angeles, Los Angeles, California 90095, USA
[3] Department of Physics, Bar-Ilan University, Ramat-Gan 52900, Israel
[4] Institute for Nanotechnology and Advanced Materials, Bar-Ilan University, Ramat-Gan 52900, Israel
[5] California NanoSystems Institute, University of California Los Angeles, Los Angeles, California 90095, USA

Note: This paper is part of the JCP Special Topic on the Ever-Expanding Optics of Single-Molecules and Nanoparticles.
[a)]**Author to whom correspondence should be addressed:** sweiss@chem.ucla.edu

ABSTRACT

We review the development of "single" nanoparticle-based inorganic and organic voltage sensors, which can eventually become a viable tool for "non-genetic optogenetics." The voltage sensing is accomplished with optical imaging at the fast temporal response and high spatial resolutions in a large field of view. Inorganic voltage nanosensors utilize the Quantum Confined Stark Effect (QCSE) to sense local electric fields. Engineered nanoparticles achieve substantial single-particle voltage sensitivity (~2% $\Delta\lambda$ spectral Stark shift up to ~30% $\Delta F/F$ per 160 mV) at room temperature due to enhanced charge separation. A dedicated home-built fluorescence microscope records spectrally resolved images to measure the QCSE induced spectral shift at the single-particle level. Biomaterial based surface ligands are designed and developed based on theoretical simulations. The hybrid nanobiomaterials satisfy anisotropic facet-selective coating, enabling effective compartmentalization beyond non-specific staining. Self-spiking- and patched-HEK293 cells and cortical neurons, when stained with hybrid nanobiomaterials, show clear photoluminescence intensity changes in response to membrane potential (MP) changes. Organic voltage nanosensors based on polystyrene beads and nanodisk technology utilize Fluorescence (Förster) Resonance Energy Transfer (FRET) to sense local electric fields. Voltage sensing FRET pairs achieve voltage sensitivity up to ~35% $\Delta F/F$ per 120 mV in cultures. Non-invasive MP recording from individual targeted sites (synapses and spines) with nanodisks has been realized. However, both of these QCSE- and FRET-based voltage nanosensors yet need to reach the milestone of recording individual action potentials from individual targeted sites.

I. INTRODUCTION

The membrane potential (MP), V_m, defined as the difference in the electrostatic potential between the interior and the exterior of a cell, is essential for the survival of living species.[1] MP acts as an energy source ("battery"), providing the cell with free energy that could be utilized for chemical and mechanical work.[2] The physical origin of MP is associated with (a) differential permeability of the ions across the membrane lipid bilayer (via ion channels and pumps), creating electrochemical gradients; (b) presence of fixed charge entities (DNAs, RNAs, and proteins) inside the cell or on its membrane boundary; and (c) asymmetric surface potential on either side of the membrane (due to charged lipid head groups).[1,3,4] Maintaining MP homeostasis is crucial for ensuring the normal functioning of various cellular processes such as energy conversion, nutrient uptake, environmental sensing, cell motility, and responses to cell stress.[5,6] Interestingly, in specialized, "excitable" cells such as neurons, cardiomyocytes, and skeletal muscle cells, MP exhibits a unique fast dynamical response in the form of "action potential" (AP). In these cells, dynamic MP changes contribute

toward information processing, communication and signaling, and muscle contraction.[7,8] Moreover, changes in MP influence (perhaps dictate) a range of physiological processes such as cellular proliferation, cellular differentiation, cell division, DNA synthesis, cell cycle progression, wound healing, and even progression of diseases such as cancer.[9]

Electrochemical communication between neurons is the basis of brain function, encompassing learning, thoughts, feelings, memories, and behaviors of living species—all mediated by APs.[10] Much of modern neurobiology stands upon the electrophysiological recordings of the activity of a single neuron embedded within a network context.[11] The neurons communicate via APs that induce the release and sensing of chemical neurotransmitters at synapses. The generation and propagation of AP signals involve asymmetric voltage depolarization and repolarization events, where MP changes from ~−70 mV (resting state) to ~+50 mV (depolarized state).[12,13] Temporally, AP is a brief (~>1 ms) electrical pulse (but varies between cell types and species).[14]

Direct measurement of electrical potential changes across the membrane has been successfully achieved, utilizing the patch-clamp electrodes or with microelectrode arrays (MEA).[15–17] These techniques offer very high sensitivity and temporal response of sub-milliseconds (ms). However, these methods of measurement are highly invasive and not suitable for simultaneous measurement from a large assembly of neuronal cells or spatially distinct sub-cellular regions within a single neuron, i.e., synapses, axons, and dendritic spines with volumes (dimensions) smaller than 1 femtoliter (~1 μm).

Another approach for measuring MPs relies on a sensor that transduces any changes in the electrical potential into some other types of signals such as fluorescence.[18] This approach is much less invasive. A bright enough fluorescent probe, by virtue of the molecular dimension, allows for imaging MP changes in multiple cells or sub-cellular regions.

Optical imaging with Ca^{2+}-sensitive fluorescent sensors is a rather popular method for sensing cellular/neuronal electrical activities.[19,20] The electrical activity is often directly correlated with the oscillations of intracellular calcium ion (Ca^{2+}) concentrations. However, Ca^{2+}-imaging is limited by its slow kinetic response (almost an order of magnitude slower than the intrinsic neuronal electrical activity, i.e., several ms vs ~>1 ms). This slow response is very slow for AP detection. In addition, since the Ca^{2+}-imaging could be influenced by other intracellular signaling processes, it does not accurately report on MP changes alone. Finally, being an indirect measurement, it requires an additional step of calibration for the optical-to-electrical signal conversion.

Recently, improved optical imaging methods have been used for understanding the information processing principles in the brain. These techniques constitute a separate field of research known as optical electrophysiology.[21] Rapid developments of various voltage sensing probes such as organic voltage-sensing dyes (VSDs),[22–24] protein-based genetically encoded voltage indicators (GEVIs),[25–28] and hybrid sensors[29,30] (combination of VSDs with GEVIs) have assisted optical electrophysiology research to flourish to a great extent. Very recently, Arch-derived Voltron GEVIs display ΔF/F as high as ~50% per 100 mV with a fast kinetic response.[s] However, GEVIs routinely exhibit a relative photoluminescence (PL) intensity change (ΔF/F) of up to ~20% for 100 mV potential change. The genetic targeting ability benefited GEVIs to probe specific subcellular locations. Over the past few years, nanoparticle (NP)-based fluorescent voltage sensors emerged very rapidly and show promise toward becoming a "non-genetic optogenetic" tool to work with wild-type cells.

To better understand how neuronal activity leads to brain functions, functional mapping of neural circuits in the brain is necessary. This would correlate local changes in MP with specific biological processes. Toward this end, additional tools and probes need to be developed to allow their investigation at the nanoscale level. Hence, the ultimate task would be to visualize/record/image the electrical activity *in vivo* (e.g., in a live mammalian brain) in a large field of view (e.g., individual action potentials from multiple neurons simultaneously) with the fast temporal response and high (super-) spatial resolutions over a long duration, non-invasively, in the behaving animal.

This review is not meant to be comprehensive nor does it cover all of the powerful (and more mature) optical voltage sensing technologies that have been already put into excellent use. Rather, it summarizes our recent efforts toward nano-scale, super-resolved voltage sensing with (i) quantum dots (QDs), (ii) nanorods (NRs), (iii) nanobeads, and (iv) nanodisks. We emphasize that these novel nanosensors are not as of yet ready for "prime-time" but argue that their further development could render them very useful in the future.

II. INORGANIC VOLTAGE NANOSENSORS OPERATING VIA THE QUANTUM CONFINED STARK EFFECT

A. Introduction to the quantum confined Stark effect (QCSE)

Semiconductor nanoparticles (NPs) such as quantum dots (QDs) and nanorods (NRs) exhibit size, shape, and morphology-dependent photoluminescence (PL) tunability together with superior brightness, excellent photostability (much-reduced photobleaching and chemical degradation as compared to organic dyes), and multiplexing ability.[31,32] As a result of these advantageous physicochemical characteristics, these materials have become a popular fluorophore for bioimaging. Moreover, the optical response of semiconductor NPs shows significant sensitivity toward changes in the local immediate environment (such as pH, temperature, dielectric, and surface charge).[33–36]

A QD/NR could sense local electric fields via the Quantum Confined Stark Effect (QCSE) (see Fig. 1).[37–41] The spatial separation of photoexcited charge carriers (electron and hole) in a confined nanostructure results in the creation of a dipole. The dipole's (opposing) response to the external electric field leads to (i) further or reduced charge separation (depending on symmetry and field direction) and (ii) changes in the exciton binding energy (Stark effect) under confinement. As a result, spectral and temporal optical responses get altered. Now, the weaker the electron–hole Coulomb interaction (implicating the smaller magnitude of the squared overlap integral "f" between the electron and hole wave functions and reduced exciton binding energy) in a material, the larger the extent of charge separation and effective polarizability under the external electric field. The effect is manifested in the form of a larger magnitude of spectral Stark shift ($\Delta\lambda$), i.e., enhanced QCSE. The physical dimension of the material also affects the extent of charge separation proportionately. A larger induced

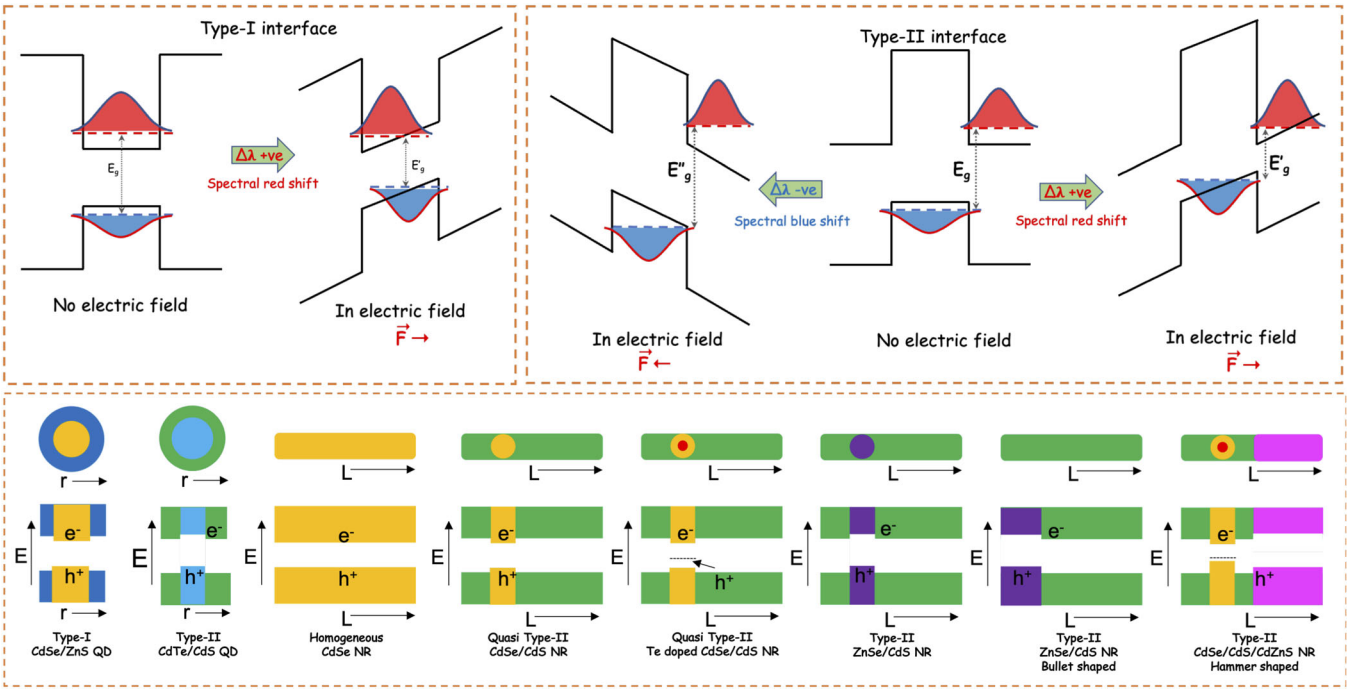

FIG. 1. The top panel shows schematics for the QCSE effect in type-I vs type-II nanoparticles. The bottom panel shows schematics of the energy band diagram for different engineered nanoparticle compositions. Reproduced with permission from Park *et al.*, ACS Nano **6**, 10013 (2012). Copyright 2012, American Chemical Society and reproduced with permission from Kuo *et al.*, ACS Photonics **5**, 4788 (2018). Copyright 2018, American Chemical Society.

internal electric field as well results in a larger magnitude of $\Delta\lambda$. In a non-homogeneous/heterostructured NP, relative band alignment influences the induced internal electric field. QCSE also affects the non-radiative Auger recombination rate (k_A) and thus strongly influences relative emission intensity changes. Another implication of enhanced charge separation, as observed experimentally, is a relative decrease in radiative lifetime ($\Delta\tau_r/\tau_r$). The associated spectral and lifetime changes can essentially be used to monitor the applied field. QCSE was first demonstrated in two-dimensional (epitaxially grown) layers of a quantum well, a strongly confined nanostructure, and was applied to electro-optical modulation devices.[42] In NPs, QCSE is commonly observed only at cryogenic temperatures.[38,43–45]

B. Room temperature QCSE at the single-particle level

At room temperature (RT), the local electric field around the nanoparticle fluctuates significantly. This interference jeopardizes charge separation modulation, resulting in spectral diffusion and broadening, thus making the RT measurements noisier and more difficult. Charge carrier trapping at the substrate, the surface of the NP, and internal interfaces with trap states aided by thermal excitations is a major contributing factor for altering the local potential around the NP. These heterogeneity induced complications could only be resolved with single-particle voltage sensing.

Single-particle QCSE induced spectral and temporal changes have been utilized to measure the local (nano-scale) electric field in various systems but most importantly for this review to measure changes in the cellular membrane potential under physiologically relevant conditions. To accomplish this, a first semiconductor NP based single particle voltage nanosensor [or voltage-sensing NP (vsNP)] has been developed by exploiting the principles of shape modifications and bandgap engineering,[46–49] and then, the nanosensor's surface is modified with biomaterials to achieve cell membrane insertion.

C. Development of materials and measurement techniques for QCSE nanosensors

1. Tools and methods

For all practical purposes, the most convenient method for visualizing MP changes *in vivo* would be to monitor the relative emission intensity changes ($\Delta I/I$) of the sensors in an acquired wide-field movie. Toward that direction, appropriate *in vitro* imaging techniques have been developed first and then extended toward *in vivo* measurements. The performance of vsNP's has been assessed in terms of QCSE sensitivity. The efficiency of QCSE is judged based on three experimental observables for individual single particles: (i) PL spectral (Stark) shift ($\Delta\lambda$); (ii) change in relative PL intensity ($\Delta F/F$); and (iii) change in PL spectral width (γ_{fwhm}). The task demands the development of modified microscopes for spectral

image acquisition. The vsNP's, deposited on custom-designed electrodes, are subjected to an externally applied electric field of strength 400 kV/cm to induce QCSE. If a 400 kV/cm electric field is being applied across a ~4 nm thick plasma membrane, that would result in a ~160 mV change in MP. In neurons, the amplitude of an AP is of the order of ~120 mV change in MP. Therefore, the applied external electric field used for assessment of vsNP's closely resembles the electric field the vsNP is supposed to experience *in vivo* such as the firing of an AP in a neuron. An imaging-based high throughput, *in vitro* screening setup, and analysis protocol for QCSE induced $\Delta\lambda$ measurements at the single nanoparticle level have been developed. The technique also enables iterative testing and optimization of synthetic protocols. One needs to understand the challenge in measuring QCSE induced $\Delta\lambda$ at the single-particle level to realize the worthiness of the tools in use. The typical width of the PL emission spectrum of single NPs is of the order of ~ tens of nm, whereas the magnitude of QCSE induced $\Delta\lambda$ is of the order of ~ a few nm, which is at least an order of magnitude smaller than γ_{fwhm}. The challenge is to detect and resolve quantitatively only a few nm of shift. The experimental setup includes (i) photolithographically patterned[50] or vertically stacked[51] electrodes with NPs in between them (see more details in the following) and (ii) a fluorescence microscope to record spectral images.

Park *et al.* used a photolithographically patterned interdigitated horizontal microelectrode containing cover glass as a screening assay.[50] Dielectrophoresis method has been utilized, during deposition, to align the NR long-axis along the field direction. This would maximize the QCSE signal. Kuo *et al.* used a "sandwiched" device, fabricated as a vertical stack of components.[51] The device essentially consists of thin-film microelectrodes with NPs "sandwiched" in between. This allows for the application of a homogeneous electric field vertically. Vertically stacked devices perform relatively better in comparison to the horizontally patterned devices due to (i) lesser extent of photobleaching (caused by photo-oxidation) for the deposited NPs and (ii) reduced number of damaging arc discharge/meltdown events.

Spectral image acquisition has been achieved with home built wide-field microscopes that allow for spectrally resolved detection of single-particle PL (see Fig. 2). Prism disperses individual point spread functions (PSFs) into spectrally resolved lines.[50,51] PL is recorded for multiple single NPs simultaneously under modulated voltage conditions (alternating from 0-to-400 kV/cm frame to frame consecutively). The camera acquisition clock (frame-rate) has been synchronized to the voltage modulation frequency. Thus, successive synchronized acquisitions of camera frames under V_{On} (400 kV/cm) and V_{Off} (0 kV/cm) conditions could have been performed. The camera records a movie containing spectral images. The spectral image of each single NP has been transformed into a calibrated spectrum for each NP, utilizing a wavelength calibration procedure for each pixel. The spectra have been fitted to a Lorentzian to find the peak wavelength. Therefore, each image frame offers PL spectrum, peak PL wavelength, and integrated PL intensity for each NP present in the field of view. It should be remembered that depending on the relative orientation between the deposited NP's polarization axis (depends on the fabrication procedure) and direction of the external electric field, experimental QCSE observables are

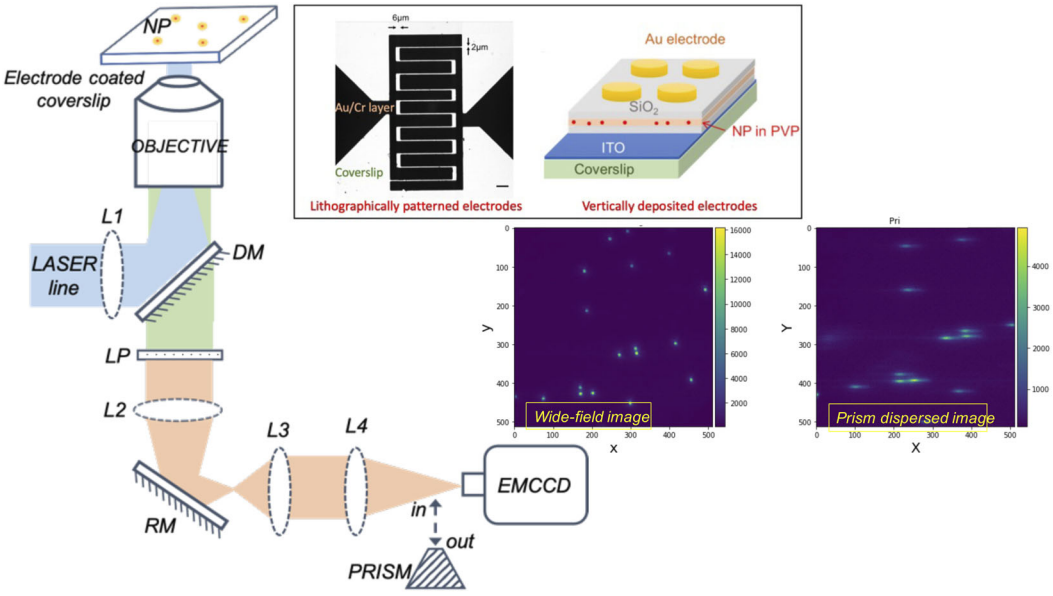

FIG. 2. Schematics of the wide-field spectrally resolved microscope. DM: dichroic mirror, L1-L4: lenses, LP: long pass filter, RM: reflective mirror, and EMCCD: electron-multiplying charged couple device. When the prism is inserted into the optical path, individual point spread functions (PSFs) coming from single NPs get dispersed into spectrally resolved lines. For QCSE measurements, the EMCCD acquisition is synchronized to an externally applied square wave voltage pulse. Inset: the top panel showing lithographically patterned and vertically deposited electrode design. Inset: the bottom panel showing wide-field and prism dispersed images. Reproduced with permission from Park *et al.*, ACS Nano **6**, 10013 (2012). Copyright 2012, American Chemical Society and reproduced with permission from Kuo *et al.*, ACS Photonics **5**, 4788 (2018). Copyright 2018, American Chemical Society.

significantly affected. Park *et al.*[50] calculated average spectra over the whole movie for V_{On} (400 kV/cm) and V_{Off} periods. $\Delta\lambda$ and $\Delta F/F$ are then computed from the average spectra. Notably, Kuo *et al.*[51] explored a different approach for quantification. From the recorded movie of spectral images, integrated intensity- and spectral peak wavelength-traces and ultimately $\Delta\lambda$ and $\Delta F/F$ traces are generated. A "burst" search algorithm is applied to these traces to extract relatively large responses. Single-particle voltage sensitivities have been quantified in terms of histograms (weighted by the total intensity counts) of $\Delta\lambda$ and $\Delta F/F$ with voltage modulations and fitted with the Gaussian function.

2. Screening for maximal QCSE sensitivity

Bandgap engineering extended the reach of PL tunability beyond the size and shape. Bandgap engineering is realized by creating a core–shell type heterostructured interface. The Synthesized materials have the ability to adjust the amplitude and spatial distribution of electron and hole wave function over the physical dimension of nanostructure. This results in modulation of the confinement potential and thus electronic coupling (overlap integral). The extent of electronic coupling ultimately controls the charge carrier separation, localization, and recombination as well as the extent and efficacy of the charge carrier's interaction with its immediate local environment. For example, in a type-II nanostructure, the band energy minima for electron and hole are spatially separated at the interface, which essentially restricts charge-carrier recombination probability and enhances charge-carrier separation probability in comparison to a type-I nanostructure. The greater the extent of separation of photoexcited charge carriers, the larger the extent of QCSE induced changes in the optical response that would be expected.

Park *et al.*[50,52,53] and Kuo *et al.*[51] engineered NPs intending to achieve substantial QCSE, ensured by enhanced charge separation at room temperature (RT). The effort involves iterative optimization of reaction conditions (precursor, injection temperature, and growth temperature). The heterostructure design has been tuned synthetically in terms of shape, composition (multi-component materials), shell thickness, relative core–shell band alignment, and doping.[33,44,54–61] The attempted synthetic modifications introduce asymmetry, (a) spatially (via shape modification, QD → NR), (b) energetically (via bandgap engineering, straddling bandgap type-I and staggered bandgap type-II). In Secs. II C 2 a–II C 2 f, we will understand the effect of synthetic modifications in terms of QCSE sensitivity.

a. Core/shell QD. The spherical QDs are isotropic in confinement. Thus, the excitonic dipole is small and isotropic. As a result, type-I (CdSe/ZnS) and quasi type-I QDs (CdS/CdSe/CdS) show not so significant $\Delta\lambda$ ~1.5–2 nm. Even for pure type-II CdTe/CdS QDs, $\Delta\lambda$ is ~3 nm. A negligible change in $\Delta\lambda$ ongoing from type-I to type-II QDs suggests that the extent of increase in charge separation due to bandgap engineering alone is not adequate for the enhancement of QCSE sensitivity. Due to the spherical symmetry, QDs show identical responses (spectral redshift only) irrespective of the direction of the externally applied field.

b. Homogeneous NR. Cylindrically symmetrical homogeneous CdSe NR also responds toward the externally applied electric field very weakly, resulting in a very small $\Delta\lambda$. The NR displays $\Delta\lambda$ ~ <4 nm (0.3%) together with $\Delta F/F$ (quenching) ~16% and ~13% spectral broadening. Again, shape modification alone is not enough to result in enhanced QCSE sensitivity. The external electric field-induced band bending is minimal, causing small perturbation to the existing strong Coulomb interaction.

c. Seeded NR. When a QD seed is positioned asymmetrically inside an elongated NR, the resulting non-homogeneous seeded NR shows anisotropic confinement. The combination of spatial and energetic asymmetry results in a relatively large and directional excitonic dipole. The directional nature of the dipole imposes an asymmetric response (positive and negative $\Delta\lambda$ and $\Delta F/F$), depending upon the direction of the externally applied electric field.

d. Quasi type-II seeded NR. A CdS NR with a CdSe QD seed inside results into a quasi-type-II heterostructure and manifests a slightly larger $\Delta\lambda$ ~4.4 nm (0.8%) along with $\Delta F/F$ (quenching) ~30% and ~28% spectral broadening. Te-doped CdSe/CdS displays similar QCSE sensitivity. Quasi type-II interface weakens Coulomb interaction due to reduced overlap integral, resulting in effectively larger charge separation and polarizability.

e. Pure type-II seeded NR—Spectral response. Type-II band alignment significantly reduces the overlap integral. Thus, in a pure type-II NR, both spatial and energetic asymmetry factors are optimal. The elongated spatial dimension of the rod in combination with asymmetric type-II band alignment causes enhanced charge separation. As anticipated, QCSE induced spectral red ($+\Delta\lambda$) and blue ($-\Delta\lambda$) shifts have been observed for these materials. The spectral blue shift should be associated with narrowing of γ_{fwhm} and enhancement of PL intensity.

For "rod"-shaped type-II ZnSe/CdS seeded NR, Kuo *et al.*[51] could achieve $\Delta\lambda$ ~3.8 nm with $\Delta F/F$ (quenching) ~42% and $\Delta\lambda$ ~(−)4.3 nm with $\Delta F/F$ (enhancement) ~69%. With the same material but a further shape modification from "rod" to "bullet," Park *et al.*[50] accomplished a greater extent of optical voltage response. For the "bullet"-shaped ZnSe/CdS seeded NR, $\Delta\lambda$ ~8 nm and ~(−)7 nm could have been observed by Park *et al.*,[50] which is significant considering the magnitude. Now, spatial and energetic asymmetry is further extended by creating a "hammer"-shaped Te doped CdSe/CdS/CdZnSe particle (see Fig. 3). This particle displays the largest QCSE, exhibiting $\Delta\lambda$ ~13 nm (2.1%) with $\Delta F/F$ (quenching) ~30% and ~30% spectral broadening as well as $\Delta\lambda$ ~(−)7 nm along with spectral narrowing, PL enhancement.[50]

Park *et al.*[50] also probed field dependence of QCSE, where external electric fields varied from −400 to +400 kV/cm. Both "hammer" and "bullet"-shaped asymmetric type-II seed NR showed nearly linear $\Delta\lambda$–F relationship, indicating symmetry breaking, whereas type-I NR, quasi type-II NR, and type-II QD showed quadratic $\Delta\lambda$–F relationship.

f. Pure type-II seeded NR—Temporal response. The temporal response time of a vsNP is just as important a characteristic parameter as spectral changes. To report and resolve fast transients such as APs, the response time following any voltage changes has to be extremely fast. An optimal voltage sensor is expected to have a sub-ms temporal response time and photon emission rate high enough [a dominant radiative exciton recombination pathway and high photoluminescence quantum yield (PLQY)] to result in sufficient signal-to-noise ratio (SNR) to record AP changes.

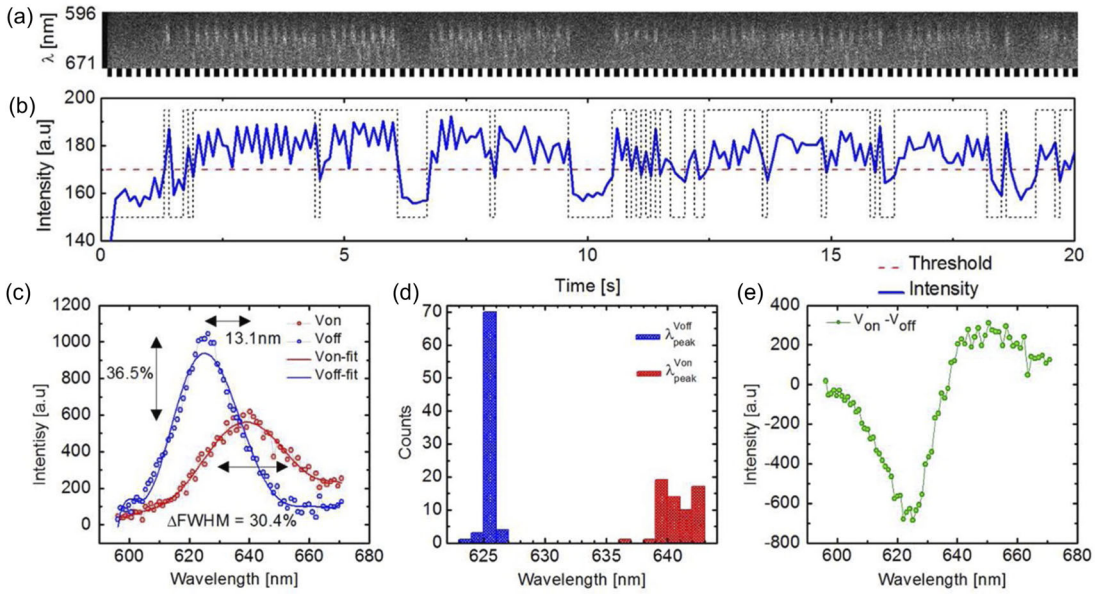

FIG. 3. Single NP's QCSE analysis of Te doped CdSe/CdS/CdZnSe NR. (a) A series of 200 successive spectra obtained from single NR at RT (excitation intensity 2 mW/cm^2, electric field modulation frequency 10 Hz, and single frame integration of 0.1 s). The dashed white/black line at the bottom of the figure indicates the periods at which the applied electric field was on (V_{on} = 400 kV/cm, white) or off (V_{off} = 0 kV/cm, black). (b) Integrated intensity trajectory (integration over λ for each frame) of the data is shown in a solid blue line. The dashed red line is a guide to the eye, emphasizing the blinking-on and blinking-off intensity states. (c) Averaged V_{on} frames (red) and averaged V_{off} frames (blue) (after filtering for frames in the blinking-on state) with corresponding seventh order polynomial fits (solid red and blue, respectively). (d) Histogram of spectral peak positions (V_{on}, red and V_{off}, blue) from all blinking-on frames (derived from the polynomial fits). (e) Differential emission spectra derived from (c). Reproduced with permission from Park *et al.*, ACS Nano **6**, 10013 (2012). Copyright 2012, American Chemical Society.

To temporally resolve PL intensity changes in response to voltage modulations, a custom spectral splitting dual-view microscope equipped with a wide-field photon counting camera (PCC) is used by Kuo *et al.*[51] The PCC can record each photon arrival time (~156 ps temporal response) and location (~50 μm spatial resolution) as well as define post-acquisition frame duration. Registration of precise photon timing allows the user to bin data from "frames" of duration much shorter than the conventional camera-based imaging. The photon counts are accumulated as a function of photon arrival time with respect to the voltage trigger (with 0-to-400 kV/cm modulation @ frequency 500 Hz and camera acquisition @ frequency 1 kHz). With the reassigned time bin 2 μs in a single modulation period, fitted accumulation trace yielded response time constants t_1 ~3.5 μs and t_2 ~8.8 μs for the rising and falling edges of photon count-time traces for type-II ZnSe/CdS seeded NR (photon emission rate ~30 kHz). The response time is orders of magnitude (~30 times) faster than that desired for resolving an AP. Bar-Elli *et al.*[62] improved upon the temporal sensitivity for spectral shift measurements. The aim is to record "fast" and "small." To achieve this, a dual detector based "balanced" detection setup is employed. PL intensity fluctuations ΔF and lifetime fluctuation $\Delta\tau$ have been measured simultaneously. The $\Delta\lambda$ has been numerically extracted from the value of the wavelength shift estimator $\Delta\Lambda$ (calculated from the simulated emission spectrum). The value of the estimator depends on the ratio of PL intensity recorded in two independent detectors in the presence and absence of the electric field. The wavelength shift estimator ($\Delta\Lambda$), a unitless parameter, is converted into the real wavelength shift in nm by comparing experimental data with the simulated data. Type-II ZnSe/CdS seeded NR (photon emission rate ~105 Hz) subjected to various electric field strengths (100–625 kV/cm, modulation @ frequency 500 Hz, and camera acquisition @ frequency 1 kHz) and different field directions. The numerical calculation yields $\Delta\lambda$ ranging from 7.1 to (−)5.5 nm. One should remember that a conventional measurement of a single NP spectrum requires much longer exposures (~1 to 10 s), which is not suitable when detecting rapid spectral shifts. The designed system proved its capability to detect small spectral shifts in response to transient/rapid (1 kHz) voltage changes with the data acquired on ms timescales.

Quite interestingly, the PL lifetime fluctuations have been observed to be correlated with QCSE induced spectral shifts for ZnSe/CdS seeded NR. Due to the small exposure duration (1 ms), photon flux is very small. Thus, lifetime is best determined by taking the mean of the photon arrival time. ZnSe/CdS NRs exhibit a biexponential PL decay pattern in the absence of an external electric field. It is the long lifetime component that mostly gets affected by the presence of the external electric field. The PL lifetime remains positively correlated with the spectral shift, i.e., spectral redshift leads to lengthening of PL lifetime and spectral blue shift accompanied by shortening of PL lifetime.

Overall, experimentally, the absolute magnitude of average optical voltage response shows that among different NPs, pure

type-II seeded NRs display maximized QCSE sensitivity, closely followed by quasi type-II seeded NR in comparison to type-I/type-II core/shell QDs as well as homogeneous NRs. Quasi type-II and type-II seeded NRs could potentially be used as voltage nanosensors, capable of reporting MP changes, with observable spectral shifts on the single-particle level.

D. Theoretical predictions for membrane-inserted voltage nanosensors

The ability of an NP to report/sense MP has been predicted theoretically by Park and Weiss[52] The NP's interaction with the external electric field has been described using quantum mechanical perturbation theory. The calculations for QCSE have been performed under the configuration where an NR is embedded symmetrically within the membrane. The calculation involves numerically solving the Schrödinger–Poisson equation under self-consistent field approximation. By solving the equation for a given dielectric distribution, an electrostatic potential profile for the NR could be obtained. The dielectric distribution represents MP, which, in turn, acts as an external electric field perturbation for the NR. The electrostatic potential profile for the NR represents the local internal electric field experienced by the NR in response to MP. Using this potential profile, electrons' and holes' wave functions and their ground state energies for different electric field strengths have been computed. With these information, $\Delta\lambda$, f, and k_A have been estimated for different external electric field perturbations. Additionally, experimentally observable QCSE parameters, i.e., relative change in fluorescence intensity ($\Delta I/I$), the relative change in a radiative lifetime ($\Delta\tau_r/\tau_r$), and the relative change in radiometric observable $\Delta I_{R/B}$ (based on $\Delta\lambda$ and γ_{fwhm}), have been determined theoretically for a physiologically relevant range of MP change, which mimics the action potential of neurons (−70 to +50 mV). CdSe NR and ZnSe/CdS seeded NR have been used for the theoretical study.

Theoretical calculations clearly showed that pure type-II seeded NR yields a larger magnitude $\Delta\lambda$ in comparison to homogeneous NR of similar length for a given applied field strength. This is because of the order of magnitude weaker Coulomb interaction. As the length increases, the extent of charge separation increases; thus, the sensitivity of QCSE increases for both types of NRs, however with a considerably greater extent for type II seeded NR. In terms of numbers, for 12 nm-sized type-I CdSe NR, theoretically obtained $\Delta\lambda$ (<1.5 nm) is negligible, whereas for 12 nm-sized type-II ZnSe/CdS NR, theoretically obtained $\Delta\lambda$ is 14.5 nm and $\Delta I_{R/B}$ is ~259% coupled with $\Delta\tau_r/\tau_r$ being (decrease) ~204% and $\Delta I/I$ being (decrease) ~98% and $\Delta\lambda$ is (−)13.8 and $\Delta I_{R/B}$ is ~(−)66% nm coupled with $\Delta\tau_r/\tau_r$ being (increase) ~70% and $\Delta I/I$ being (increase) ~40% per 100 mV. Notably, a 100 mV of MP change across a 4 nm thick membrane bilayer is equivalent to the 250 kV/cm external electric field experienced by the NR. These calculations, in principle, serve as a guideline of maximum MP sensitivity in terms of different observables when NRs are embedded into the membrane symmetrically and vertically. The degree of insertion has a major impact on the observed effective voltage sensitivity. For any other configuration, where NR is being inserted with canting angle ($\theta > 0$) to membrane normal direction ($\theta = 0$), the actual internal electric field would be reduced, which, in turn, reduces the effective voltage sensitivity of the probe.

1. Correlation between probe insertion geometry and QCSE sensitivity—Experimental support

Kuo *et al.* experimentally probed the effect of the relative orientation of the emission transition dipole concerning the direction of the externally applied electric field and the extent QCSE induced spectral Stark shift for type II ZnSe/CdS seeded NR (see Fig. 4).[51] The defocused image of a single emitter displays characteristic interference patterns that contain information about the three-dimensional orientation of the molecule. Patra *et al.*[63,64] developed a defocused imaging microscopy technique and analysis algorithm for pattern matching for yielding orientation geometry. Defocused images could be obtained with minimal but precise movement of the optics (objective movement with a piezoelectric transducer) toward the single emitter (negative z-direction) in a standard wide-field microscope. Emission spectra and orientation geometry (based on defocused images) for randomly oriented NRs are measured experimentally. As the angle between the emission transition dipole and the applied electric field decreases, the $\Delta\lambda$ increases. The voltage sensitivity is highest when the emission transition dipole is almost parallel to the applied electric field and is lowest for an orthogonal arrangement between the two.

Overall, theoretical simulation of external electric field-induced changes in photophysical properties as a function of the heterostructured interface and geometry qualitatively mimics experimental results[51,52] and entrusts utilization of type-II vsNPs for *in vivo* MP sensing measurements.

E. Cellular delivery, membrane insertion, and MP sensing with QCSE voltage nanosensors

Integrating NPs into biological and neuroscience applications is one of the major obstacles to overcome. Synthesized NPs, without any surface modifications, are not suitable to use directly in biological systems particularly because of NP's undefined surface properties, which often result in nonspecific binding. Effective MP sensing demands for effective membrane targeting and insertion of the probe. This has been achieved via NP's anisotropic facet-selective surface functionalization with biomaterials, which enables better control over the insertion orientation. The resulting hybrid nanobiomaterials perform better than the pure inorganic or biomaterial. The component biomaterial imparts membrane protein-like properties to the hybrid material. The hybrid nanobiomaterials are water-soluble, biologically active, undergo bimolecular recognition, and could be engineered to have improved renal clearance. Biomolecular recognition refers to specific noncovalent bonding interactions happening between different biomolecular structures. This specific interaction results in the stable and spontaneous insertion of the hybrid material into the membrane lipid bilayer. Careful design of the biomaterial used for surface coating of vsNPs allows attaining more control over spatial alignment in specific biological space. As a result, these hybrid nanobiomaterials have recently become increasingly popular probes for *in vivo* molecular imaging, intracellular biological imaging, single protein tracking in live cells, and most importantly biosensing.

Nevertheless, a careful trade-off between the magnitude of QCSE sensitivity (increasing with NR size) and the efficacy of membrane insertion (decreasing with increasing NR size) is also

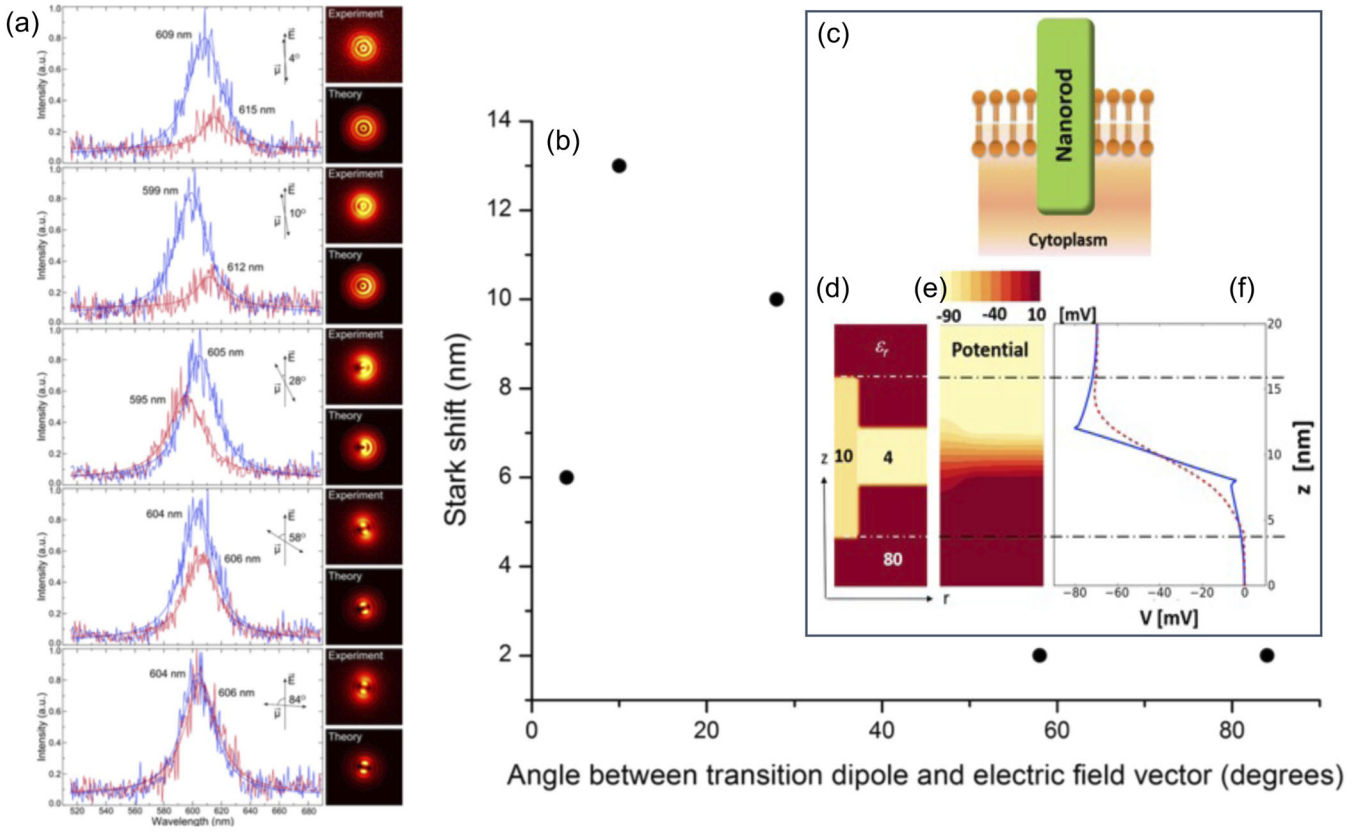

FIG. 4. (a) Emission spectra of five randomly oriented type-II ZnSe/CdS NRs in the presence and absence of the applied electric field. The orientations of the emission transition dipoles of these NRs are shown as μ by black arrows, and the direction of the applied electric field is shown as E. The images acquired by defocused imaging experimentally and theoretically are shown on the right. (b) The QCSE spectral shift as a function of the angle between the emission transition dipole and the applied electric field. The inset shows calculated potential of the inserted NR in the membrane. (c) Schematic of NR embedded in the membrane. (d) Dielectric constants: ε_r, intra- and extracellular, 80 (red); lipid, 4 (yellow); and NR, 10 (dark yellow). The ε_r-values at the boundaries and interfaces are averaged. (e) Color map of the calculated potential profile of geometry when Vm = 70 mV. (f) One-dimensional potential profile across the NR (dashed red line) and outside of the NR (solid blue line). (Dashed-dotted black lines) Top and bottom of the NR. Reproduced with permission from Kuo *et al.*, ACS Photonics **5**, 4788 (2018). Copyright 2018, American Chemical Society and reproduced with permission from K. Park and S. Weiss, Biophys. J. **112**, 703 (2017). Copyright 2017, Author(s), licensed under a Creative Commons Attribution (CC-BY-NC-ND) license.

necessary. The optimal voltage sensor should have large detectable voltage sensitivity while maintaining a small material dimension for effective membrane insertion. It has been shown theoretically by Park and Weiss[52] that seeded NRs having length <12 nm with aspect ratio >1.5 exhibit significant *in vivo* QCSE sensitivity and gets inserted into the membrane relatively easily. The optimal orientation for the NR inside the membrane would be the NR's long axis aligned parallel to the membrane's normal with both ends of the NR symmetrically extruding the membrane on both sides, i.e., tips/ends being exposed to the cytoplasm and extracellular matrix, respectively. Having this insertion orientation stable is a very challenging task. The complexity of the job further escalates due to the "rod" shape of the probe, which has differential curvature ("top" vs "side"). This would call for a non-homogeneous coating design to tackle the varying curvatures of the surfaces.

1. Peptide coated quasi type-II seeded NR

Park *et al.*[53] designed alpha-helical flexible peptide as surface ligand, which satisfies the facet selective non-homogeneous coating principle (see Fig. 5). The binding of the peptide to the NRs is mediated by cystine residues. Strategically, the peptide is so designed that it contains more hydrophilic amino acids (structurally flexible, yield better fit to the edges) to cover the top surface of the rod, whereas more hydrophobic/lipophilic amino acids cover (structurally rigid helical domain) the sides of the rod. The hydrophobic region of the surface covering dictates the partitioning of the peptide coated NRs (pcNRs) into the membrane. A quasi type-II CdSe/CdS seeded NR, covered with ~8–12 peptides, has been used. The designed sequence of the peptide allowed the hybrid nanobiomaterials to localize themselves at the membrane–water interface,

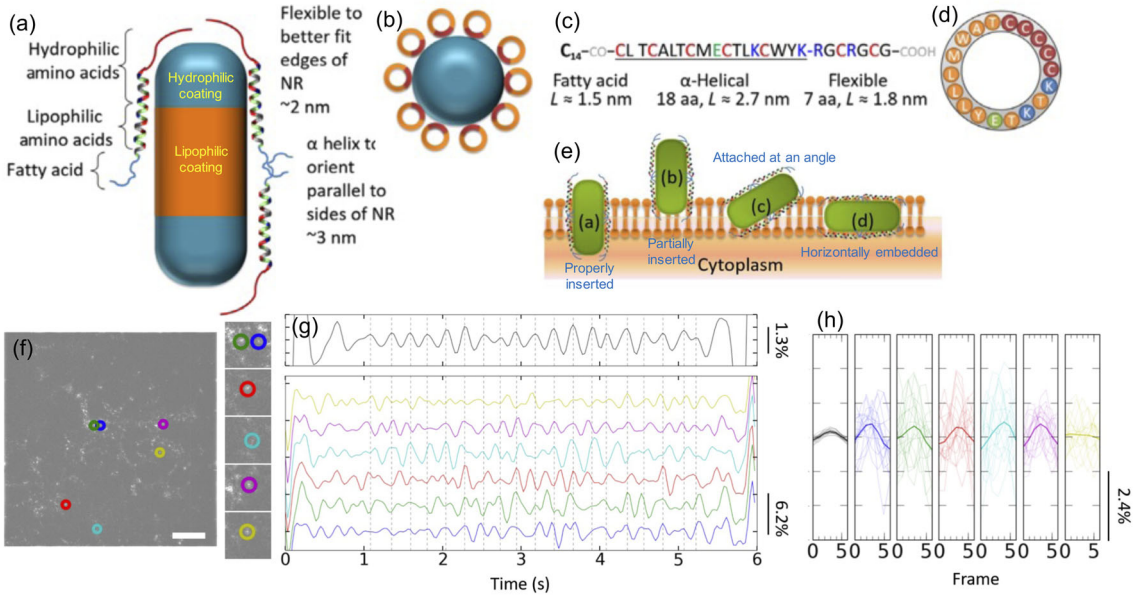

FIG. 5. (a) Schematic cartoon describing surface functionalization with peptide for rendering NR. This functionalization will impart membrane protein-like properties to the NR, favoring its stable, spontaneous insertion into the membrane with proper orientation. (b) Top view of an NR coated with peptide surface ligand. Brown and orange colors depict Cys-rich and lipophilic faces of the α-helical peptide, respectively. (c) The sequence of the designed peptide. C14–CO- stands for the myristoyl acid residue attached to the N-terminal amino group. (d) Wheel diagram corresponding to the a-helical part of the peptide. Color coding is the same as in (a). (e) Schematics of possible pcNR association with the lipid bilayer. (f) Fluorescence image of spiking HEK293 cells stained with pcNRs. A spatially high-pass filter is applied to the image to highlight signals from individual pcNRs and remove background signals. (g) Temporal bandpass-filtered $\Delta F/F$ time trace (19 consecutive cycles and 7 frames per cycle) of single/small aggregates of pcNRs from (f). The gray line in the top panel represents ensemble average response. (h) $\Delta F/F$ response around every local maximum in the trajectory. The mean $\Delta F/F$'s over 23 cycles are plotted with thicker lines. The gray line in the leftmost panel represents the ensemble average response. Reproduced with permission from Park *et al.*, Sci. Adv. **4**, e1601453 (2018). Copyright 2018, Author(s), licensed under a Creative Commons Attribution (CC-BY-NC) license.

perpendicular to the membrane surface. Simulation for the energetics of NR's membrane insertion as a function of the canting angle suggests that if the length of the hydrophobic surfaces covering remains comparable to the membrane thickness, a significant fraction of rods gets inserted into the membrane with minimal canting angle (~10°). At the same time, the hydrophilic ends of the peptide (covering NR tips) stabilize the orientation of the rod embedded within the membrane. Experimentally, the efficiency of membrane insertion for the peptide design could be asserted from the association of pcNRs with model membrane vesicles that resemble the membrane lipid bilayer. The cryoEM micrographs show that ~16% of the total SUVs (small unilamellar vesicles) are loaded with appropriately inserted probes. Among them, ~34% of these pcNRs undergo desired perpendicular insertion and ~42% of the pcNRs undergo partially tilted insertion in SUVs. Further, polarization microscopy measurements indicate that ~58% of these pcNRs undergo more or less perpendicular insertion in electro-swelled GUVs (giant unilamellar vesicles). Attainment of a sizable fraction of preferred vertical insertion suggests the feasibility of utilization for this surface functionalization approach. Park *et al.* applied pcNRs to probe the electrical activity in self-spiking HEK293 (self-oscillation @ 3–4 Hz) as well as non-spiking wild-type HEK293 cells. For self-spiking HEK293 cells, PL intensity fluctuations in response to MP fluctuations could be observed clearly. However, in terms of magnitude, the sensing sensitivity is not impressive. The $\Delta F/F$ turns out to be ~1% for the ensemble and as high as ~5% for single particles. Moreover, only ~16% of single particles exhibits $\Delta F/F > 1\%$. For wild-type HEK293 cells, voltage sensing experiments are carried out using an "optical electrophysiology" setup. This is essentially a home-built wide-field microscope, equipped to perform simultaneous whole-cell patch-clamp recordings together with fluorescence imaging. The MP of the probed cell has been modulated through an attached patched electrode. PL movies recorded (frame rate @ 400 Hz) in coordination with the MP modulation [voltage modulation frequency @ 100 Hz and voltage fluctuating between 0 and (−)150 mV]. pcNRs present in patched cells showed modulated responses (calculated from PL intensity bursts), which are distinguishable in comparison to signals from pcNRs in unpatched cells. However, due to the long integration time (30 ms/frame), AP-like events could not be resolved.

2. Lipid coated pure type-II seeded NR

Ludwig *et al.*[65] functionalized the surface of the NRs with a lipid mixture derived from the brain extract. A type-II ZnSe/CdS seeded NR has been used. Due to tissue-specific natural lipid composition, NRs get spontaneously translocated, via biological recognition, into the neuronal plasma membrane. The hydrophilic tail of the lipids interacts with the alkane chains of the nanoparticle surface ligands. The cryoEM micrograph shows ~10% of the total SUVs loaded

with lipid-coated NRs (lcNRs) with appropriate insertion, orthogonal to the membrane plane. Ludwig *et al.* applied lcNRs to probe the electrical activity in cultured cortical neurons. A home-built microscope setup, capable of carrying out wide-field, spectrally split ratiometric imaging as well as simultaneous patch-clamp measurements, has been utilized. The ratiometric imaging approach allows one to measure MP changes induced optical response in terms of (i) PL intensity (ΔF, sum of the two emission channels) as well as (ii) spectral shift (ΔRt, ratio between the two emission channels). Camera acquisition (frame rate @ 100 Hz) has been synchronized with the MP modulation. The MP of neurons is modulated with the patched electrode [voltage modulation frequency @ 25 Hz and voltage fluctuating between 0 and (−)60 mV]. During responsive periods, ΔF/F as high as 40% and ΔRt as high as 0.1 (corresponding to Δλ ~5 nm) could be observed. However, for the selected intervals, averaged ΔF/F is ~10% and ΔRt is ~0.01 (corresponding to Δλ ~0.6 nm), which is not impressive enough. In fact, within a given defined time trace, brief periods of moderate-to-significant voltage-sensitive responses interrupted by intervals of weak or no voltage response ultimately result in overall poor averaged out voltage sensitivity. Notably, only 0.6% of the lcNRs shows responsiveness toward MP modulations. These short "bursts" of responsiveness are perhaps because of transient membrane insertion events. Less than expected stability of insertion and orientation is perhaps the reason for the experimentally observed reduced voltage sensitivity of NRs. It should be remembered that the cellular plasma membrane composition is relatively more complex in comparison to SUV and GUV, which results in lower effective *in vivo* insertion.

III. ORGANIC VOLTAGE NANOSENSORS OPERATING VIA FLUORESCENCE RESONANCE ENERGY

A. Introduction to fluorescence resonance energy transfer (FRET)

Förster resonance energy transfer (FRET) is a non-radiative energy transfer process between an excited state of molecule donor fluorophore to another acceptor fluorophore in proximity (<10 nm).[66] The efficiency of FRET is extremely sensitive to the spatial separation between the donor–acceptor fluorophores. Thus, FRET measurements are often utilized as an efficient spectroscopic ruler for measuring distance changes between the interacting biomolecules or during conformational changes within biomolecules.[66–69] There exists a class of optical voltage sensors that relies on the principle of FRET.[70–72] The plasma membrane thickness (~5 to 10 nm) and the distance required between the donor–receptor molecules allows FRET to be an effective method for measuring membrane potential (MP). FRET measurements have been utilized for the detection of MP changes in the ensemble level and more recently in the single NP level.[73]

B. Development of materials and measurement techniques for FRET nanosensors

Voltage sensing by FRET is illustrated by the system where one of the dyes is fixed to one of the lipid leaflets (for example, dioctadecyloxacarbocyanine, DiO, a lipophilic dye that labels the membrane)—donor—and a charged, hydrophobic moiety that moves up and down in between the leaflets in response to changes in the electric field (for example, Dipicrylamine, DPA, a non-fluorescent lipophilic anion) —acceptor. Changes in the distance, which are proportionate to the changes in MP, are translated to the FRET efficiency, which could be measured via donor intensity or lifetime changes. We have recently developed and utilized nanobeads and nanodisks (NDs) as NP donors for FRET-based MP sensing. The mechanism was first reported with the oxonol derivative (donor) and a Texas Red-labeled lectin (acceptor) and inspired the development of methods for MP sensing by FRET.[74] Oxonol penetrates the membrane and is located in the outer/inner leaflet depending on the MP. The fluorophor labeled lectin is not membrane permeable and located on the outer side of the membrane (adjacent). The imaging of MP changes is a result of distance-dependent energy transfer between the two elements.[74] This technique has been used successfully to image the activity of several individual neurons in leech nerve cords during locomotion. To achieve dye penetration in this more intact preparation, a slower translocating oxonol with a time constant of 400 μs has been used.[75] In comparison, the time constant of a widely used single-component dye such as di 8-ANEPPS is about 2 μs per 100 mV at room temperature.[76,77] Additionally, an interesting hybrid voltage sensor (hVOS) approach consisting of the synthetic voltage-sensitive molecule, dipycrilamine (DPA), and a genetically expressed donor (GFP) that binds to the membrane has been developed,[81] Similar to oxonol, DPA is a lipophilic anion quencher (acceptor) molecule translocated from the inner to the outer leaflet of the membrane (and vice versa) according to the changes in MP as a response to electric field changes. It is highly voltage-sensitive in terms of rapid (<0.5 ms) spatial translocation within the cell membrane.[81] It has been reported that two-component systems that are genetically encoded allow for visualization of rapid membrane potential changes in cells and neurons.[78] Many variants for voltage sensing by FRET have been developed in recent years.[79,80] We review our development of vsNPs (nanobead- and nanodisk-based) using DPA as an acceptor in the FRET system.

1. Nanobeads

Fluorescent polystyrene (FPS) beads are commercially available with a range of uniform sizes (>~20 nm diameter) and can be loaded as spectrally suitable dyes for FRET interaction with DPA. Moreover, FPS beads can be targeted to a specific site on the cell membrane by synthesizing functional surface groups or recognition molecules. FPS beads typically have a very thin layer of surface groups, which practically bring the surface of the FPS beads to direct contact with the cell membrane and are attached to the cell membrane extracellularly from outside. The fluorophores encapsulated within the FPS bead are homogeneously distributed; the population of fluorophores closest to the membrane surface may involve in FRET interaction with DPA located within the plasma membrane. With any change in MP, negatively charged DPA molecules translocate in response between the inner and the outer leaflets. At hyperpolarizing potentials, the DPA molecules are closer to the outer leaflet of the membrane and the bead's fluorescence undergoes quenching due to increased FRET; upon depolarization, the DPA molecules are translocated toward the inner leaflet, resulting in decreased FRET, leading to fluorescence enhancement in comparison to the resting state.

Shapira *et al.* employed FPS (with a hydrodynamic diameter of ~70 nm) as hydrophilic, negatively charged surface beads in combination with DPA as FRET induced vsNPs (see Fig. 6).[82] Fluorescence response to membrane potential changes (over a range of applied voltage, −60 to +60 mV) has been demonstrated from ensemble membrane staining as well as from single NPs in HEK293 cells and primary cortical neurons. Simultaneous optical and electrical measurements (whole-cell patch-clamp) have been performed; FPS beads applied to the extracellular solution gets spontaneously adsorbed into the cell membranes (within a few minutes with no apparent cytotoxicity). The changes in fluorescence intensity are well correlated with the changes in MP. With HEK293 cells, depolarization resulted in the decline of fluorescence intensity (fluorescence beads undergo quenching) with $\Delta F/F \sim 5.6\%$ per 120 mV. The temporal response for voltage sensing using FPS bead–DPA FRET vsNP is estimated to be of the order of ~5 ms. HEK293 cells have been further labeled to achieve sparse staining. Each cell is labeled with 1–6 fluorescence spots. ~78% of the single spots showed voltage responsiveness. Single spot based analysis showed averaged $\Delta F/F \sim 3.3\%$ per 120 mV. Neurons have been sparsely labeled. Single spots located in neuron's soma probed for voltage responsiveness displayed averaged $\Delta F/F \sim 2.5\%$ per 120 mV. FPS bead–DPA FRET pair system displays adequate sensitivity to perform MP measurements from single particles.

2. Nanodisks

Recently, advances in the field of structural biology of membrane proteins have yielded nanodisk (ND) technology. This technology is based on the self-assembly of engineered biomacromolecules (likewise apo-lipoprotein and phospholipids.) into discoidal nanoparticles. NDs are relatively easy to produce, non-toxic, and biodegradable. NDs can be functionalized via their lipid headgroups or through the protein side chains, which allow the NDs to attach to the cell membrane. NDs are capable of incorporating various types of lipids and different kinds of lipophilic molecules. NDs can be loaded with lipophilic fluorescent donor dyes and anchor/attach to the cell membrane. Thus, with NDs, a FRET-based sensing mechanism could be established utilizing DPA as an acceptor.

Grupi *et al.* developed a lipid ND–DPA FRET pair system for MP sensing (see Fig. 7).[73] It consists of avidin as a steric barrier ND (with the fluorophores TopFluor and Cy5) and DPA molecules. MP measurements were performed in HEK293 cells and primary cortical neurons probed using $ND_{TF,\ Cy5}$-avidin construct in combination with a solution consisting of DPA. The fluorescence changes remain correlated with MP changes and consistent with the FRET pair system. For HEK293 cells, the averaged $\Delta F/F$ is ~33% per 120 mV. Under similar ensemble staining conditions, for neurons, the averaged $\Delta F/F$ is ~23% per 120 mV.

C. Cellular delivery, targeting, and MP sensing with FRET voltage nanosensors

For the FRET system to be effective and sensitive to specific changes in both voltage and structural changes *in vitro* and *in vivo*, different methods have been developed with various nanoparticles [QD, gold nanoparticulate, different polymers, and expression controls of fluorophore (lox/cre)]. One of many examples has been

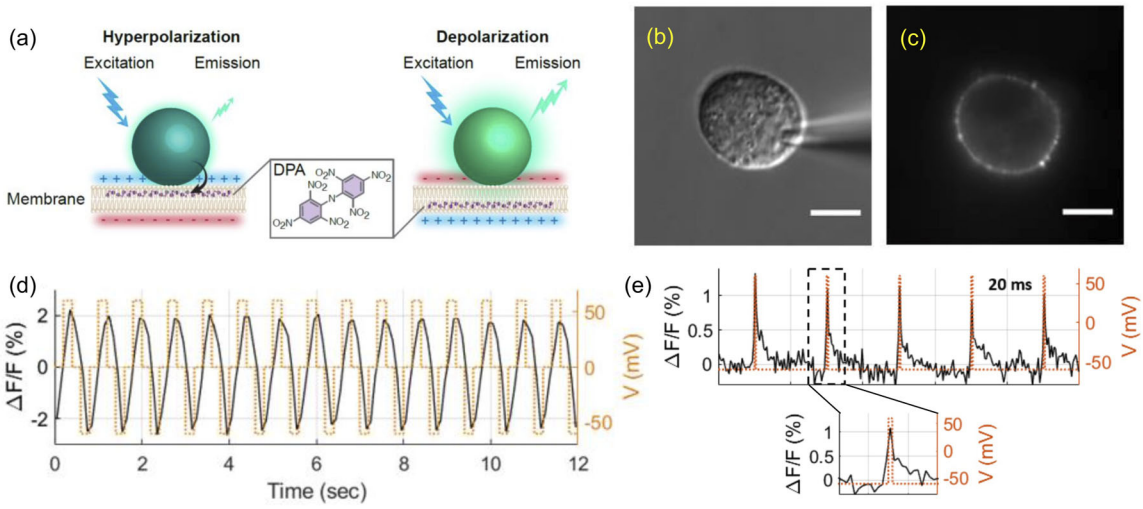

FIG. 6. (a) The FPS beads/DPA FRET pair mechanism. The FPS beads are attached to the extracellular side of the cell membrane; at hyperpolarization, DPA molecules translocate to the outer leaflet of the membrane and closer to the beads, resulting in increased FRET and a decrease in the bead's fluorescence. Upon depolarization, the DPA molecules redistribute to the inner leaflet and away from the beads, increasing the bead's fluorescence. A DIC (b) and a fluorescence (c) image of a single HEK cell in the whole-cell patch-clamp mode. The patch electrode is shown in (b). (d) The fluorescence response of FPS beads/DPA FRET pair to the membrane voltage in HEK cells. The voltage was stepped from 0 mV to either +60 or −60 mV and back to 0 mV. The duration of each step was 200 ms. (e) Response kinetics of FPS beads/DPA FRET pair to changes in the membrane voltage in HEK cells. The changes in fluorescence for 20 ms pulses, imaging at a frame rate of 50 Hz, are shown. The membrane potential was stepped from a holding potential of −60 to +60 mV. The HEK cells are labeled with 0.5 nM beads in the presence of 2 μM DPA in the bath solution. Reproduced with permission from Grupi *et al.*, Biophys. Rep. **1**, 100007 (2021). Copyright 2021, Author(s), licensed under a Creative Commons Attribution (CC-BY-NC-ND) license.

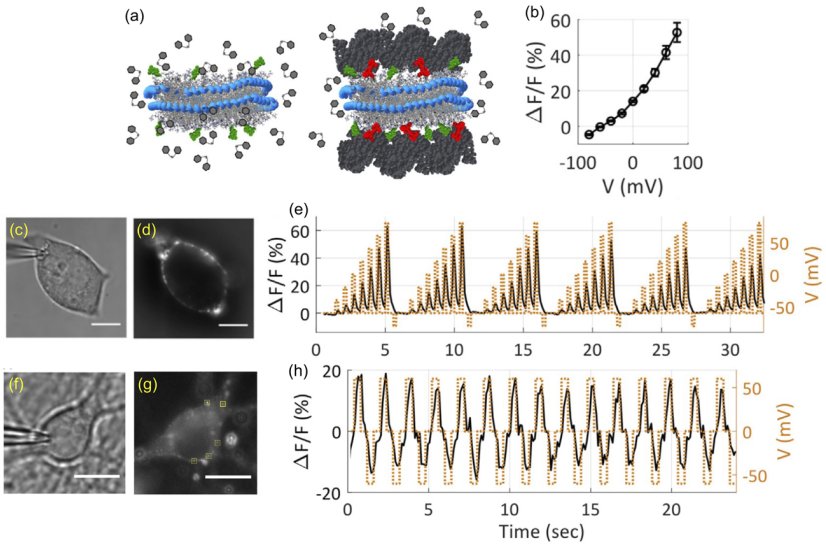

FIG. 7. (a) Schematics of functionalized NDs. NDs are labeled by TF (green) in the presence of DPA (gray hexagons). DPA is in both the solvent and the ND bilayer. NDs are labeled by TF and Cy5-PE (red). The ND bilayer surface is capped by avidin (dark gray), which restricts the distance between DPA and TF. (b) The average change in Cy5 fluorescence emission as a function of membrane potential, relative to the emission at −60 mV. The voltage waveform consisted of varying voltage levels with 20 mV steps for 200 ms at each voltage level and a 400 ms resting period of −60 mV. The optical recording was done at a 10 Hz frame rate. Middle panel—fluorescence response of NDTF, Cy5-DPA to changes in the membrane potential in HEK293 cells. Cells were stained with NDTF, Cy5 and voltage-clamped in the presence of 2 μM DPA. (c) Differential interference contrast (DIC) image and (d) Cy5 fluorescence emission of a patch-clamped HEK293 cell. Scale bars: 10 μm. (e) The signal trajectory of Cy5 fluorescence emission as a function of the membrane potential. Lower panel—fluorescence response of NDTF, Cy5-DPA to changes in the membrane potential in primary cortical neuron cells. Cells were stained with NDTF, Cy5-avidin and voltage-clamped in the presence of 2 μM DPA. (f) DIC image and (g) Cy5 fluorescence emission of a patch-clamped primary cortical neuron. Scale bars: 10 μm. The cells were clamped to a square voltage waveform consisting of 0, 60, 0, and −60 mV voltage levels, each 400 ms in duration. (h) Change in Cy5 fluorescence emission as a function of the membrane potential from NDTF, Cy5 in the region inside the solid yellow square shown in (g). Reproduced with permission from Grupi *et al*., Biophys. Rep. **1**, 100007 (2021). Copyright 2021, Author(s), licensed under a Creative Commons Attribution (CC-BY-NC-ND) license.

shown that chemical labeling of a unique cysteine, followed by enzymatic modification of reactive glutamine in an N-terminally appended substrate sequence recognition tag for transglutaminase (TGase), affords a stoichiometrically donor/acceptor-labeled protein suitable for single-molecule FRET experiments.[83] For successful application to biological systems, FRET systems should be efficient in fast transmission and should provide accurate information, such as AP within a neural network. This system must have (1) a donor with strong emission intensity and (2) a maximum overlap between the donor and acceptor with minimal overlap with the environmental molecules. Biological adaptation between the substance and the biological system is needed to avoid unwanted toxins or side effects.

The uniqueness of the nanoparticles used in the FRET system is the ability of the particles to mark a single spot in the cell or on the membrane. Hence, the ability of an active group coupling to the donor/acceptor to perform targeting to a specific site on the cellular membrane and enable voltage measurement is a unique advantage. To date, biocompatible QD conjugates have been used successfully for sentinel lymph node mapping, tumor targeting, tumor angiogenesis imaging, and metastatic cell tracking, for example, conjugating an antibody to a QD for site recognition in live cells, quantum dot labeling of live MCF-7 breast cancer epithelial cells, surface targeting of EGFR receptors with anti-EGFR (epidermal growth factor receptor) antibodies conjugated to CdSe/ZnS QDs,[83–86] and conjugating an antibody to a gold particle in order. Based on cholesterol's ability to insert into the plasma membrane, we investigate whether AuNP functionalization with linear dihydrolipoic acid–poly(ethylene) glycol (DHLA–PEG) chains distally terminated with cholesterol (AuNP–PEG–Chol) can enable light-induced AP generation in neurons. Voltage recordings under current-clamp conditions showed that DRG (Dorsal Root Ganglia) neurons labeled in this manner exhibited a capacity for AP generation in response to microsecond and millisecond pulses of 532 nm light, a property attributable to the close tethering of AuNP–PEG–Chol conjugates to the plasma membrane, facilitated by the cholesterol moiety. Light-induced AP and subthreshold depolarizing responses of the DRG neurons were similar to those previously described for AuNP conjugates targeted to channel proteins using large, multicomponent immunoconjugates.[87,88] Another great example is that $ND_{TF,Cy5}$ has been conjugated with antibody anti-$GABA_AR$ g2 via a hydrophilic linker. ABB-G is a recognition element for the $GABA_A$ receptor, which allows for targeted labeling of a specific neuron site (synapse, soma, and dendrite). Targeted ND_{TF}, $_{Cy5}$-Ab-avidin conjugated anti-$GABA_AR$ construct stained significantly better than non-targeted ND_{TF}, $_{Cy5}$-avidin.The average F/F for neurons with the targeted ND_{TF}, $_{Cy5}$-Ab-avidin construct was 35%–45%. The ability to measure the voltage from a single site on the neuron membrane using an antibody conjugated to a nanodisk is a great advantage. The ability to measure membrane voltage from a single synapse can shed light on deciphering the network activity in neurons.

IV. CONCLUSIONS AND OUTLOOK

We reviewed here our recent efforts toward developing nanoscale, super-resolved voltage sensors. We have shown that properly functionalized and bandgap engineered inorganic NPs with enhanced QCSE can be inserted into membranes and locally record the membrane potential in self-spiking- and patched-HEK293 cells and in cortical neurons (that are non-genetically manipulated). FRET-based organic NPs (beads and NDs) can also locally record the membrane potential in cultured cells and neurons and even be targeted to–and record from–a single synapse.

Further improvements are still needed to render these NPs as widely used reagents for voltage sensing. With inorganic voltage nanosensors, a notable drawback is the non-uniform, broad distribution of voltage sensitivities. Heterogeneous voltage response is arising from a range of factors such as size and shape heterogeneity of the vsNPs and active movement of the vsNPs within the membrane. Future efforts need to further improve the uniformity of NP physical properties, enhancing QCSE sensitivity and effectiveness of stable membrane insertion. To accomplish single-particle voltage response, enhanced charge separation should be counterbalanced with a good enough radiative recombination rate. The task opens up new horizons for synthesizing novel nanostructures. The possibility of functionalizing a nanoparticles' "inorganic" surface with "organic" biomolecules creates opportunities for further design and development of flexible, facet-selective bio-ligands. Strategies for environmentally triggering surface ligand distribution need to be devised. This will improve membrane insertion efficiency and mitigate issues such as dynamic orientation fluctuation for the voltage nanosensor. Fluorescence blinking (intermittency) of these particles is another problem that needs to be solved (however, blinking indicates success in reaching the single-particle level recording). With the combination of the higher photon emission rate for the ensuing vsNPs and the faster image acquisition rate (>1 KHz), recording single AP signals should be possible in the future. In addition, vsNPs could, in principle, be engineered for voltage induced PL lifetime changes and thus can be utilized in lifetime-based imaging techniques for MP sensing.

Organic voltage nanosensors (beads and NDs) also need to be further improved. A simplified non-FRET based approach could be further explored for NDs by directly incorporating VSDs. Targeting different sites using different colors and different conjugated antibodies could possibly allow for simultaneous MP recording from different targeted sites (pre- and post-synaptic membranes) within the same neuron. This will allow monitoring of the electrical activity across the (single) synapse.

Beyond high voltage sensitivity, high brightness, high localization accuracy, and targetability, these nanosensors are suited for "non-genetic optogenetics," which can then work with wild-type cells/organisms. With further developments, we hope that these voltage nanosensors could be added to the already impressive arsenal of tools for the study of the electrical activity in the brain of live behaving animals.

ACKNOWLEDGMENTS

The authors thank past and present Weiss group members contributing to the voltage nanosensors project including Dr. Asaf Grupi, Dr. Nurit Degani-Katzav, Shimon Yudovich and Lion Morgenstein at Bar Ilan University, and Dr. Kyoung Park, Dr. Yung Kuo, Dr. Antonino Ingargiola, Dr. Jack Li, and Dr. Xavier Michalet at UCLA and members of the Shvadchak group (CAS), Oron group (WIS), Enderlein group (GAUG), Ludwig group (HiLIFE), and Triller group (CNRS). This work has received funding from the European Research Council (ERC) under the European Union's Horizon 2020 research and innovation program (Grant No. NVS669941); the Human Frontier Science Program research (Grant No. RGP0061/2015); the Defense Advanced Research Projects Agency (DARPA)/Biological Technologies Office (Grant No. D14PC00141); the Biological and Environmental Research (BER) program of the Department of Energy Office of Science (Grant Nos. DE-02ER63421 and DE-SC0020338); the STROBE National Science Foundation Science and Technology Center (Grant No. DMR-1548924); the NIH (Grant Nos. 5R01EB000312 and 1R01GM086197); the United States-Israel Binational Science Foundation (Grant No. 2010382) the Israel Science Foundation (Grant No. 813/19); and the Bar-Ilan Research and Development Co., the Israel Innovation Authority (Grant No. 63392).

AUTHOR DECLARATIONS

Conflict of Interest

The authors have no conflicts to disclose.

Author Contributions

D.R. and Z.S. contributed equally to this work.

DATA AVAILABILITY

This is a review paper and does not contain any original data. The data availability statements could be found in the original papers.

REFERENCES

[1]S. H. Wright, "Generation of resting membrane potential," Adv. Physiol. Educ. **28**, 139–142 (2004).

[2]C. Brosseau and E. Sabri, "Resistor-capacitor modelling of the cell membrane: A multiphysics analysis," J. Appl. Phys. **129**, 011101 (2021).

[3]R. L. Veech, Y. Kashiwaya, and M. T. King, "The resting membrane potential of cells are measures of electrical work, not of ionic currents," Integr. Physiol. Behav. Sci. **30**, 283–307 (1995).

[4]J. Lombard, "Once upon a time the cell membranes: 175 years of cell boundary research," Biol. Direct **9**, 32 (2014).

[5]M. Chappell and S. Payne, *Physiology for Engineers: Applying Engineering Methods to Physiological Systems* (Springer, 2016), Vol. 13.

[6]J. M. Benarroch and M. Asally, "The microbiologist's guide to membrane potential dynamics," Trends Microbiol. **28**, 304–314 (2020).

[7]B. P. Bean, "The action potential in mammalian central neurons," Nat. Rev. Neurosci. **8**, 451–465 (2007).

[8]P. M. Hopkins, "Skeletal muscle physiology," Contin. Educ. Anaesth., Crit. Care Pain **6**, 1–6 (2006).

[9]L. Abdul Kadir, M. Stacey, and R. Barrett-Jolley, "Emerging roles of the membrane potential: Action beyond the action potential," Front. Physiol. **9**, 1661 (2018).

[10]D. M. Lovinger, "Communication networks in the brain neurons, receptors, neurotransmitters, and alcohol," Alcohol Res. Health **31**, 196–214 (2008).

[11]E. Neher and B. Sakmann, "The patch-clamp technique," Sci. Am. **266**, 44–51 (1992).
[12]G. Stuart, N. Spruston, B. Sakmann, and M. Häusser, "Action potential initiation and backpropagation in neurons of the mammalian CNS," Trends Neurosci. **20**, 125–131 (1997).
[13]P. M. Lalley and U. Windhorst, in *Encyclopedia of Neuroscience*, edited by U. Windhors, M. D. Binder, and N. Hirokawa (Springer, Berlin, Heidelberg, 2009), pp. 22–29.
[14]K. Holthoff, D. Zecevic, and A. Konnerth, "Rapid time course of action potentials in spines and remote dendrites of mouse visual cortex neurons," J. Physiol. **588**, 1085–1096 (2010).
[15]M. J. Mason, A. K. Simpson, M. P. Mahaut-Smith, and H. P. C. Robinson, "The interpretation of current-clamp recordings in the cell-attached patch-clamp configuration," Biophys. J. **88**, 739–750 (2005).
[16]J. Dunlop, M. Bowlby, R. Peri, D. Vasilyev, and R. Arias, "High-throughput electrophysiology: An emerging paradigm for ion-channel screening and physiology," Nat. Rev. Drug Discovery **7**, 358–368 (2008).
[17]M. E. J. Obien, K. Deligkaris, T. Bullmann, D. J. Bakkum, and U. Frey, "Revealing neuronal function through microelectrode array recordings," Front. Neurosci. **8**, 423 (2015).
[18]M. Scanziani and M. Häusser, "Electrophysiology in the age of light," Nature **461**, 930 (2009).
[19]R. M. Paredes, J. C. Etzler, L. T. Watts, W. Zheng, and J. D. Lechleiter, "Chemical calcium indicators," Methods **46**, 143–151 (2008).
[20]Y. Zhao, S. Araki, J. Wu, T. Teramoto, Y.-F. Chang, M. Nakano, A. S. Abdelfattah, M. Fujiwara, T. Ishihara, T. Nagai, and R. E. Campbell, "An expanded palette of genetically encoded Ca^{2+} indicators," Science **333**, 1888–1891 (2011).
[21]K. D. Piatkevich, E. E. Jung, C. Straub, C. Linghu, D. Park, H.-J. Suk, D. R. Hochbaum, D. Goodwin, E. Pnevmatikakis, N. Pak, T. Kawashima, C.-T. Yang, J. L. Rhoades, O. Shemesh, S. Asano, Y.-G. Yoon, L. Freifeld, J. L. Saulnier, C. Riegler, F. Engert, T. Hughes, M. Drobizhev, B. Szabo, M. B. Ahrens, S. W. Flavell, B. L. Sabatini, and E. S. Boyden, "A robotic multidimensional directed evolution approach applied to fluorescent voltage reporters," Nat. Chem. Biol. **14**, 352–360 (2018).
[22]A. Grinvald and R. Hildesheim, "VSDI: A new era in functional imaging of cortical dynamics," Nat. Rev. Neurosci. **5**, 874–885 (2004).
[23]L. M. Loew, in *Membrane Potential Imaging in the Nervous System and Heart*, edited by O. Bernus, M. Canepari, and D. Zecevic (Springer International Publishing, Cham, 2015), pp. 27–53.
[24]M. Kannan, G. Vasan, S. Haziza, C. Huang, R. Chrapkiewicz, J. Luo, J. A. Cardin, M. J. Schnitzer, and V. A. Pieribone, "Dual polarity voltage imaging reveals subthreshold dynamics and concurrent spiking patterns of multiple neuron-types," bioRxiv:10.1101/2021.10.13.463730.
[25]H. Zhang, E. Reichert, and A. E. Cohen, "Optical electrophysiology for probing function and pharmacology of voltage-gated ion channels," eLife **5**, e15202 (2016).
[26]D. R. Hochbaum, Y. Zhao, S. L. Farhi, N. Klapoetke, C. A. Werley, V. Kapoor, P. Zou, J. M. Kralj, D. MacLaurin, N. Smedemark-Margulies, J. L. Saulnier, G. L. Boulting, C. Straub, Y. K. Cho, M. Melkonian, G. K.-S. Wong, D. J. Harrison, V. N. Murthy, B. L. Sabatini, E. S. Boyden, R. E. Campbell, and A. E. Cohen, "All-optical electrophysiology in mammalian neurons using engineered microbial rhodopsins," Nat. Methods **11**, 825–833 (2014).
[27]Y. Adam, "All-optical electrophysiology in behaving animals," J. Neurosci. Methods **353**, 109101 (2021).
[28]A. S. Abdelfattah, J. Zheng, D. Reep, G. Tsegaye, A. Tsang, B. J. Arthur, M. Rehorova, C. V. Olson, Y. Huang, Y. Shuai *et al.*, "Sensitivity optimization of a rhodopsin-based fluorescent voltage indicator," bioRxiv:10.1101/2021.11.09.467909.
[29]H. H. Yang and F. St-Pierre, "Genetically encoded voltage indicators: Opportunities and challenges," J. Neurosci. **36**, 9977–9989 (2016).
[30]Y. Bando, C. Grimm, V. H. Cornejo, and R. Yuste, "Genetic voltage indicators," BMC Biol. **17**, 71 (2019).
[31]X. Michalet, F. F. Pinaud, L. A. Bentolila, J. M. Tsay, S. Doose, J. J. Li, G. Sundaresan, A. M. Wu, S. S. Gambhir, and S. Weiss, "Quantum dots for live cells, in vivo imaging, and diagnostics," Science **307**, 538–544 (2005).
[32]D. Bera, L. Qian, T.-K. Tseng, and P. H. Holloway, "Quantum dots and their multimodal applications: A review," Materials **3**, 2260–2345 (2010).
[33]J. Müller, J. M. Lupton, A. L. Rogach, J. Feldmann, D. V. Talapin, and H. Weller, "Monitoring surface charge migration in the spectral dynamics of single CdSe/CdS nanodot/nanorod heterostructures," Phys. Rev. B **72**, 205339 (2005).
[34]S. Li, K. Zhang, J.-M. Yang, L. Lin, and H. Yang, "Single quantum dots as local temperature markers," Nano Lett. **7**, 3102–3105 (2007).
[35]I. L. Medintz, M. H. Stewart, S. A. Trammell, K. Susumu, J. B. Delehanty, B. C. Mei, J. S. Melinger, J. B. Blanco-Canosa, P. E. Dawson, and H. Mattoussi, "Quantum-dot/dopamine bioconjugates function as redox coupled assemblies for *in vitro* and intracellular pH sensing," Nat. Mater. **9**, 676–684 (2010).
[36]M. Zhu, J. Zhou, Z. Hu, H. Qin, and X. Peng, "Effects of local dielectric environment on single-molecule spectroscopy of a CdSe/CdS core/shell quantum dot," ACS Photonics **5**, 4139–4146 (2018).
[37]D. A. B. Miller, D. S. Chemla, T. C. Damen, A. C. Gossard, W. Wiegmann, T. H. Wood, and C. A. Burrus, "Band-edge electroabsorption in quantum well structures: The quantum-confined Stark effect," Phys. Rev. Lett. **53**, 2173–2176 (1984).
[38]S. A. Empedocles and M. G. Bawendi, "Quantum-confined Stark effect in single CdSe nanocrystallite quantum dots," Science **278**, 2114–2117 (1997).
[39]G. W. Men, J. Y. Lin, H. X. Jiang, and Z. Chen, "Quantum-confined Stark effects in semiconductor quantum dots," Phys. Rev. B **52**, 5913–5922 (1995).
[40]J. Müller, J. M. Lupton, A. L. Rogach, J. Feldmann, D. V. Talapin, and H. Weller, "Enhanced quantum-confined Stark effect in single core-shell semiconductor nanorods," in *Conference on Lasers and Electro-Optics/Quantum Electronics and Laser Science and Photonic Applications Systems Technologies, Technical Digest (CD)* (Optica Publishing Group, 2005), paper QTuE1.
[41]R. Scott, A. W. Achtstein, A. v. Prudnikau, A. Antanovich, L. D. A. Siebbeles, M. Artemyev, and U. Woggon, "Time-resolved Stark spectroscopy in CdSe nanoplatelets: Exciton binding energy, polarizability, and field-dependent radiative rates," Nano Lett. **16**, 6576–6583 (2016).
[42]D. Miller, D. Chemla, T. Damen, T. Wood, C. Burrus, A. Gossard, and W. Wiegmann, "The quantum well self-electrooptic effect device: Optoelectronic bistability and oscillation, and self-linearized modulation," IEEE J. Quantum Electron. **21**, 1462–1476 (1985).
[43]E. Rothenberg, M. Kazes, E. Shaviv, and U. Banin, "Electric field-induced switching of the fluorescence of single semiconductor quantum rods," Nano Lett. **5**, 1581–1586 (2005).
[44]J. Müller, J. M. Lupton, P. G. Lagoudakis, F. Schindler, R. Koeppe, A. L. Rogach, J. Feldmann, D. V. Talapin, and H. Weller, "Wave function engineering in elongated semiconductor nanocrystals with heterogeneous carrier confinement," Nano Lett. **5**, 2044–2049 (2005).
[45]Y. Xing, L. Wang, D. Yang, Z. Wang, Z. Hao, C. Sun, B. Xiong, Y. Luo, Y. Han, J. Wang, and H. Li, "A novel model on time-resolved photoluminescence measurements of polar InGaN/GaN multi-quantum-well structures," Sci. Rep. **7**, 45082 (2017).
[46]A. M. Smith and S. Nie, "Semiconductor nanocrystals: Structure, properties, and band gap engineering," Acc. Chem. Res. **43**, 190–200 (2010).
[47]J. A. Smyder and T. D. Krauss, "Coming attractions for semiconductor quantum dots," Mater. Today **14**, 382 (2011).
[48]H. Zhu and T. Lian, "Wavefunction engineering in quantum confined semiconductor nanoheterostructures for efficient charge separation and solar energy conversion," Energy Environ. Sci. **5**, 9406–9418 (2012).
[49]Y. Nandan and M. S. Mehata, "Wavefunction engineering of type-I/type-II excitons of CdSe/CdS core-shell quantum dots," Sci. Rep. **9**, 2 (2019).
[50]K. Park, Z. Deutsch, J. J. Li, D. Oron, and S. Weiss, "Single-molecule quantum-confined Stark effect measurements of semiconductor nanoparticles at room temperature," ACS Nano **6**, 10013–10023 (2012).
[51]Y. Kuo, J. Li, X. Michalet, A. Chizhik, N. Meir, O. Bar-Elli, E. Chan, D. Oron, J. Enderlein, and S. Weiss, "Characterizing the quantum-confined Stark effect in semiconductor quantum dots and nanorods for single-molecule electrophysiology," ACS Photonics **5**, 4788–4800 (2018).
[52]K. Park and S. Weiss, "Design rules for membrane-embedded voltage-sensing nanoparticles," Biophys. J. **112**, 703–713 (2017).
[53]K. Park, Y. Kuo, V. Shvadchak, A. Ingargiola, X. Dai, L. Hsiung, W. Kim, H. Zhou, P. Zou, A. J. Levine, J. Li, and S. Weiss, "Membrane insertion of–and membrane potential sensing by-semiconductor voltage nanosensors: Feasibility demonstration," Sci. Adv. **4**, e1601453 (2018).

[54]R. Xie, U. Kolb, J. Li, T. Basché, and A. Mews, "Synthesis and characterization of highly luminescent CdSe–core CdS/$Zn_{0.5}Cd_{0.5}S$/ZnS multishell nanocrystals," J. Am. Chem. Soc. **127**, 7480–7488 (2005).
[55]D. V. Talapin, J. H. Nelson, E. V. Shevchenko, S. Aloni, B. Sadtler, and A. P. Alivisatos, "Seeded growth of highly luminescent CdSe/CdS nanoheterostructures with rod and tetrapod morphologies," Nano Lett. **7**, 2951–2959 (2007).
[56]Z. Deng, H. Yan, and Y. Liu, "Bandgap engineering of quaternary-alloyed ZnCdSSe quantum dots via a facile phosphine-free colloidal method," J. Am. Chem. Soc. **131**, 17744–17745 (2009).
[57]H. Zhu, N. Song, and T. Lian, "Wave function engineering for ultrafast charge separation and slow charge recombination in type II core/shell quantum dots," J. Am. Chem. Soc. **133**, 8762–8771 (2011).
[58]N. N. Hewa-Kasakarage, M. Kirsanova, A. Nemchinov, N. Schmall, P. Z. El-Khoury, A. N. Tarnovsky, and M. Zamkov, "Radiative recombination of spatially extended excitons in (ZnSe/CdS)/CdS heterostructured nanorods," J. Am. Chem. Soc. **131**, 1328–1334 (2009).
[59]O. Chen, J. Zhao, V. P. Chauhan, J. Cui, C. Wong, D. K. Harris, H. Wei, H.-S. Han, D. Fukumura, R. K. Jain, and M. G. Bawendi, "Compact high-quality CdSe–CdS core-shell nanocrystals with narrow emission linewidths and suppressed blinking," Nat. Mater. **12**, 445–451 (2013).
[60]D. Roy, T. Routh, A. V. Asaithambi, S. Mandal, and P. K. Mandal, "Spectral and temporal optical behaviour of blue-, green-, orange-, and red-emitting CdSe-based core/gradient alloy shell/shell quantum dots: Ensemble and single-particle investigation results," J. Phys. Chem. C **120**, 3483–3491 (2016).
[61]D. Mocatta, G. Cohen, J. Schattner, O. Millo, E. Rabani, and U. Banin, "Heavily doped semiconductor nanocrystal quantum dots," Science **332**, 77–81 (2011).
[62]O. Bar-Elli, D. Steinitz, G. Yang, R. Tenne, A. Ludwig, Y. Kuo, A. Triller, S. Weiss, and D. Oron, "Rapid voltage sensing with single nanorods via the quantum-confined Stark effect," ACS Photonics **5**, 2860–2867 (2018).
[63]D. Patra, I. Gregor, and J. Enderlein, "Image analysis of defocused single-molecule images for three-dimensional molecule orientation studies," J. Phys. Chem. A **108**, 6836–6841 (2004).
[64]D. Patra, I. Gregor, J. Enderlein, and M. Sauer, "Defocused imaging of the quantum-dot angular distribution of radiation," Appl. Phys. Lett. **87**, 101103 (2005).
[65]A. Ludwig, P. Serna, L. Morgenstein, G. Yang, O. Bar-Elli, G. Ortiz, E. Miller, D. Oron, A. Grupi, S. Weiss, and A. Triller, "Development of Lipid-coated semiconductor nanosensors for the recording of membrane potential in neurons," ACS Photonics **7**, 1141–1152 (2020).
[66]E. Lerner, T. Cordes, A. Ingargiola, Y. Alhadid, S. Chung, X. Michalet, and S. Weiss, "Toward dynamic structural biology: Two decades of single-molecule Förster resonance energy transfer," Science **359**(6373), eaan1133 (2018).
[67]B. Hellenkamp, S. Schmid, O. Doroshenko, O. Opanasyuk, R. Kühnemuth, S. Rezaei Adariani, B. Ambrose, M. Aznauryan, A. Barth, V. Birkedal, M. E. Bowen, H. Chen, T. Cordes, T. Eilert, C. Fijen, C. Gebhardt, M. Götz, G. Gouridis, E. Gratton, T. Ha, P. Hao, C. A. Hanke, A. Hartmann, J. Hendrix, L. L. Hildebrandt, V. Hirschfeld, J. Hohlbein, B. Hua, C. G. Hübner, E. Kallis, A. N. Kapanidis, J.-Y. Kim, G. Krainer, D. C. Lamb, N. K. Lee, E. A. Lemke, B. Levesque, M. Levitus, J. J. McCann, N. Naredi-Rainer, D. Nettels, T. Ngo, R. Qiu, N. C. Robb, C. Röcker, H. Sanabria, M. Schlierf, T. Schröder, B. Schuler, H. Seidel, L. Streit, J. Thurn, P. Tinnefeld, S. Tyagi, N. Vandenberk, A. M. Vera, K. R. Weninger, B. Wünsch, I. S. Yanez-Orozco, J. Michaelis, C. A. M. Seidel, T. D. Craggs, and T. Hugel, "Precision and accuracy of single-molecule FRET measurements—A multi-laboratory benchmark study," Nat. Methods **15**, 669–676 (2018).
[68]D. K. Sasmal, L. E. Pulido, S. Kasal, and J. Huang, "Single-molecule fluorescence resonance energy transfer in molecular biology," Nanoscale **8**, 19928–19944 (2016).
[69]J. C. Sanders and E. D. Holmstrom, "Integrating single-molecule FRET and biomolecular simulations to study diverse interactions between nucleic acids and proteins," Essays Biochem. **65**, 37–49 (2021).
[70]H. Mutoh, A. Perron, D. Dimitrov, Y. Iwamoto, W. Akemann, D. M. Chudakov, and T. Knöpfel, "Spectrally-resolved response properties of the three most advanced FRET-based fluorescent protein voltage probes," PLoS One **4**, e4555 (2009).
[71]P. Zou, Y. Zhao, A. D. Douglass, D. R. Hochbaum, D. Brinks, C. A. Werley, D. J. Harrison, R. E. Campbell, and A. E. Cohen, "Bright and fast multicoloured voltage reporters via electrochromic FRET," Nat. Commun. **5**, 4625 (2014).
[72]Y. Gong, M. J. Wagner, J. Zhong Li, and M. J. Schnitzer, "Imaging neural spiking in brain tissue using FRET-opsin protein voltage sensors," Nat. Commun. **5**, 3674 (2014).
[73]A. Grupi, Z. Shapira, S. Yudovich, N. Degani-Katzav, and S. Weiss, "Point-localized, site-specific membrane potential optical recording by single fluorescent nanodiscs," Biophys. Rep. **1**, 100007 (2021).
[74]J. T. Robinson, M. Jorgolli, A. K. Shalek, M.-H. Yoon, R. S. Gertner, and H. Park, "Vertical nanowire electrode arrays as a scalable platform for intracellular interfacing to neuronal circuits," Nat. Nanotechnol. **7**, 180–184 (2012).
[75]T. W. Cacciatore, P. D. Brodfuehrer, J. E. Gonzalez, T. Jiang, S. R. Adams, R. Y. Tsien, W. B. Kristan, Jr., and D. Kleinfeld, "Identification of neural neuro techniques circuits by imaging coherent electrical activity with FRET-based dyes," Neuron **23**, 449–459 (1999).
[76]R. S. Bedlack, M.-D. Wei, S. H. Fox, E. Gross, and L. M. Loew, "Distinct electric potentials in soma and neurite membranes," Neuron **13**, 1187–1193 (1994).
[77]S. Rohr and B. M. Salzberg, "Multiple sites optical recording of transmembrane voltage (MSORTV) in patterned growth heart cell cultures: Assessing electrical behaviour, with microsecond resolution, on a cellular and subcellular scale," Biophys. J. **67**, 1301–1315 (1994).
[78]B. Chanda, R. Blunck, L. C. Faria, F. E. Schweizer, I. Mody, and F. Bezanilla, "A hybrid approach to measuring electrical activity in genetically specified neurons," Nat. Neurosci. **8**, 1619–1626 (2005).
[79]U. Sung, M. Sepehri-Rad, H. H. Piao, L. Jin, T. Hughes, L. B. Cohen, and B. J. Baker, "Developing fast fluorescent protein voltage sensors by optimizing FRET interactions," PLoS One **10**(11), e0141585 (2015).
[80]Y. Ma, P. O. Bayguinov, and M. B. Jackson, "Optical studies of action potential dynamics with hVOS probes," Sci. Rep. **9**, 15878 (2019).
[81]Y. Ma, P. O. Bayguinov, and M. B. Jackson, "Optical studies of action potential dynamics with hVOS probes," Curr. Opin. Biomed. Eng. **12**, 51–58 (2019).
[82]Z. Shapira, N. Degani-Katzav, S. Yudovich, A. Grupi, and S. Weiss, "Optical probing of local membrane potential with fluorescent polystyrene beads," Biophys. Rep. (published online 2021).
[83]G. Iyer, J. Xu, and S. Weiss, "Single-step conjugation of antibodies to quantum dots for labelling cell surface receptors in mammalian cells," Methods Mol. Biol. **751**, 553–563 (2011).
[84]N. Tjahjono, Y. Jin, A. Hsu, M. Roukes, and L. Tian, "Letting the little light of mind shine: Advances and future directions in neurochemical detection," Neurosci. Res. (published online 2021).
[85]T. Goris, D. P. Langley, P. R. Stoddart, and B. del Rosal, "Nanoscale optical voltage sensing in biological systems," J. Lumin. **230**, 117719 (2021).
[86]J. L. Carvalho-de-Souza, O. K. Nag, E. Oh, A. L. Huston, I. Vurgaftman, D. R. Pepperberg, F. Bezanilla, and J. B. Delehanty, "Cholesterol functionalization of gold nanoparticles enhances photoactivation of neural activity," ACS Chem. Neurosci. **10**, 1478–1487 (2019).
[87]N.-T. Chen, S.-H. Cheng, C.-P. Liu, J. Souris, C.-T. Chen, C.-Y. Mou, and L.-W. Lo, "Recent advances in nanoparticle-based Förster resonance energy transfer for biosensing, molecular imaging and drug release profiling," Int. J. Mol. Sci. **13**, 16598–16623 (2012).
[88]A. Denizli, *Molecular Imprinting for Nanosensors and Other Sensing Application* (Elsevier (2021).